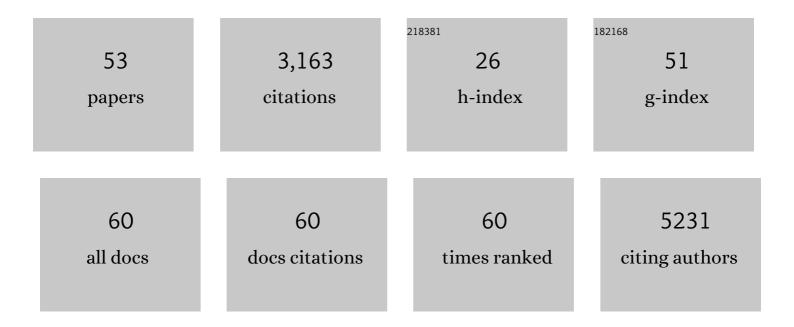
Xiaoke Mu

List of Publications by Year in descending order

Source: https://exaly.com/author-pdf/7809924/publications.pdf Version: 2024-02-01



XIAOKE MIL

#	Article	IF	CITATIONS
1	Singleâ€Layered Ultrasmall Nanoplates of MoS ₂ Embedded in Carbon Nanofibers with Excellent Electrochemical Performance for Lithium and Sodium Storage. Angewandte Chemie - International Edition, 2014, 53, 2152-2156.	7.2	826
2	"Nanoâ€Pearl‧tring―TiNb ₂ O ₇ as Anodes for Rechargeable Lithium Batteries. Advanced Energy Materials, 2013, 3, 49-53.	10.2	220
3	Hollow Carbon Nanospheres with a High Rate Capability for Lithiumâ€Based Batteries. ChemSusChem, 2012, 5, 400-403.	3.6	215
4	An FeF ₃ ·0.5H ₂ O Polytype: A Microporous Framework Compound with Intersecting Tunnels for Li and Na Batteries. Journal of the American Chemical Society, 2013, 135, 11425-11428.	6.6	177
5	Fast Li Storage in MoS ₂ â€Grapheneâ€Carbon Nanotube Nanocomposites: Advantageous Functional Integration of 0D, 1D, and 2D Nanostructures. Advanced Energy Materials, 2015, 5, 1401170.	10.2	155
6	Top-Down Synthesis of Open Framework Fluoride for Lithium and Sodium Batteries. Chemistry of Materials, 2013, 25, 962-969.	3.2	117
7	Fast kinetics of multivalent intercalation chemistry enabled by solvated magnesium-ions into self-established metallic layered materials. Nature Communications, 2018, 9, 5115.	5.8	114
8	A Highâ€Capacity Cathode for Lithium Batteries Consisting of Porous Microspheres of Highly Amorphized Iron Fluoride Densified from Its Open Parent Phase. Advanced Energy Materials, 2013, 3, 113-119.	10.2	111
9	Tailoring Surface Frustrated Lewis Pairs of In ₂ O _{3â^'} <i>_x</i> (OH) _y for Gasâ€Phase Heterogeneous Photocatalytic Reduction of CO ₂ by Isomorphous Substitution of In ³⁺ with Bi ³⁺ . Advanced Science. 2018. 5. 1700732.	5.6	91
10	VOCI as a Cathode for Rechargeable Chloride Ion Batteries. Angewandte Chemie - International Edition, 2016, 55, 4285-4290.	7.2	81
11	Cu-Zr nanoglasses: Atomic structure, thermal stability and indentation properties. Acta Materialia, 2017, 136, 181-189.	3.8	78
12	Lithium/Oxygen Incorporation and Microstructural Evolution during Synthesis of Liâ€Rich Layered Li[Li _{0.2} Ni _{0.2} Mn _{0.6}]O ₂ Oxides. Advanced Energy Materials, 2019, 9, 1803094.	10.2	78
13	Macroscopic nanodiamonds/β-SiC composite as metal-free catalysts for steam-free dehydrogenation of ethylbenzene to styrene. Applied Catalysis A: General, 2015, 499, 217-226.	2.2	53
14	Radial distribution function imaging by STEM diffraction: Phase mapping and analysis of heterogeneous nanostructured glasses. Ultramicroscopy, 2016, 168, 1-6.	0.8	52
15	Nanodiamond decorated few-layer graphene composite as an efficient metal-free dehydrogenation catalyst for styrene production. Catalysis Today, 2015, 249, 167-175.	2.2	45
16	Mapping structure and morphology of amorphous organic thin films by 4D-STEM pair distribution function analysis. Microscopy (Oxford, England), 2019, 68, 301-309.	0.7	45
17	Multichannel hollow TiO2 nanofibers fabricated by single-nozzle electrospinning and their application for fast lithium storage. Electrochemistry Communications, 2013, 28, 54-57.	2.3	43
18	A highly N-doped carbon phase "dressing―of macroscopic supports for catalytic applications. Chemical Communications, 2015, 51, 14393-14396.	2.2	43

Χιάοκε Μυ

#	Article	IF	CITATIONS
19	Structure and Properties of Nanoglasses. Advanced Engineering Materials, 2018, 20, 1800404.	1.6	42
20	Evolution of order in amorphous-to-crystalline phase transformation of MgF ₂ . Journal of Applied Crystallography, 2013, 46, 1105-1116.	1.9	39
21	Towards quantitative treatment of electron pair distribution function. Acta Crystallographica Section B: Structural Science, Crystal Engineering and Materials, 2019, 75, 532-549.	0.5	38
22	Unveiling the Local Atomic Arrangements in the Shear Band Regions of Metallic Glass. Advanced Materials, 2021, 33, e2007267.	11.1	38
23	Lithium Potential Variations for Metastable Materials: Case Study of Nanocrystalline and Amorphous LiFePO ₄ . Nano Letters, 2014, 14, 5342-5349.	4.5	33
24	Highâ€Performance Lowâ€Temperature Li ⁺ Intercalation in Disordered Rockâ€Salt Li–Cr–V Oxyfluorides. ChemElectroChem, 2016, 3, 892-895.	1.7	32
25	Solution Growth of Ultralong Gold Nanohelices. ACS Nano, 2017, 11, 5538-5546.	7.3	30
26	Understanding the graphitization and growth of free-standing nanocrystalline graphene using in situ transmission electron microscopy. Nanoscale, 2017, 9, 12835-12842.	2.8	27
27	(De)Lithiation Mechanism of Hierarchically Layered LiNi _{1/3} Co _{1/3} Mn _{1/3} O ₂ Cathodes during High-Voltage Cycling. Journal of the Electrochemical Society, 2019, 166, A5025-A5032.	1.3	27
28	VOCl as a Cathode for Rechargeable Chloride Ion Batteries. Angewandte Chemie, 2016, 128, 4357-4362.	1.6	26
29	Surface segregation of primary glassy nanoparticles of Fe90Sc10 nanoglass. Materials Letters, 2016, 181, 248-252.	1.3	23
30	Revealing the Dual Surface Reactions on a HE-NCM Li-Ion Battery Cathode and Their Impact on the Surface Chemistry of the Counter Electrode. ACS Applied Materials & Interfaces, 2019, 11, 6054-6065.	4.0	23
31	Electron Beam Effects on Oxide Thin Films—Structure and Electrical Property Correlations. Microscopy and Microanalysis, 2019, 25, 592-600.	0.2	23
32	Interlayerâ€Expanded Vanadium Oxychloride as an Electrode Material for Magnesiumâ€Based Batteries. ChemElectroChem, 2017, 4, 738-745.	1.7	22
33	Activation and degradation of electrospun LiFePO4 battery cathodes. Journal of Power Sources, 2018, 396, 386-394.	4.0	21
34	Structural Evolution of Magnesium Difluoride: from an Amorphous Deposit to a New Polymorph. Inorganic Chemistry, 2011, 50, 1563-1569.	1.9	20
35	Secondâ€Harmonic Generation from ZnO/Al ₂ O ₃ Nanolaminate Optical Metamaterials Grown by Atomic‣ayer Deposition. Advanced Optical Materials, 2016, 4, 1203-1208.	3.6	19
36	Mechanical Milling Assisted Synthesis and Electrochemical Performance of High Capacity LiFeBO ₃ for Lithium Batteries. ACS Applied Materials & Interfaces, 2016, 8, 2166-2172.	4.0	18

Χιάοκε Μυ

#	Article	IF	CITATIONS
37	Grain boundary segregation induced precipitation in a non equiatomic nanocrystalline CoCuFeMnNi compositionally complex alloy. Acta Materialia, 2021, 220, 117281.	3.8	18
38	Tuning the Curie temperature of Fe90Sc10 nanoglasses by varying the volume fraction and the composition of the interfaces. Scripta Materialia, 2019, 159, 109-112.	2.6	13
39	Unveiling local atomic bonding and packing of amorphous nanophases via independent component analysis facilitated pair distribution function. Acta Materialia, 2021, 212, 116932.	3.8	13
40	Quantifying the performance of a hybrid pixel detector with GaAs:Cr sensor for transmission electron microscopy. Ultramicroscopy, 2021, 227, 113298.	0.8	12
41	Spectroscopic investigations on the origin of the improved performance of composites of nanoparticles/graphene sheets as anodes for lithium ion batteries. Carbon, 2018, 127, 47-56.	5.4	11
42	Influence of a Second Cation (<i>M</i> = Ca ²⁺ , Mg ²⁺) on the Phase Evolution of (Ba <i>_xM</i> _{1–<i>x</i>})F ₂ Starting from Amorphous Deposits. Zeitschrift Fur Anorganische Und Allgemeine Chemie, 2014, 640, 1868-1875.	0.6	10
43	Role of surface spins on magnetization of Cr2O3 coated Î ³ -Fe2O3 nanoparticles. Solid State Sciences, 2018, 83, 43-48.	1.5	10
44	Investigating hybridization schemes of coupled split-ring resonators by electron impacts. Optics Express, 2015, 23, 20721.	1.7	7
45	New Insight into Desodiation/Sodiation Mechanism of MoS ₂ : Sodium Insertion in Amorphous Mo–S Clusters. ACS Applied Materials & Interfaces, 2021, 13, 40481-40488.	4.0	7
46	Reversible control of magnetism: on the conversion of hydrated FeF ₃ with Li to Fe and LiF. Journal of Materials Chemistry A, 2019, 7, 24005-24011.	5.2	6
47	Low temperature structural stability of Fe ₉₀ Sc ₁₀ nanoglasses. Materials Research Letters, 2018, 6, 178-183.	4.1	4
48	Solar Fuels: Tailoring Surface Frustrated Lewis Pairs of In ₂ O _{3â^'} <i>_x</i> (OH) _y for Gasâ€Phase Heterogeneous Photocatalytic Reduction of CO ₂ by Isomorphous Substitution of In ³⁺ with Bi ³⁺ (Adv. Sci. 6/2018). Advanced Science, 2018, 5, 1870034.	5.6	3
49	Radial Distribution Function Imaging by Diffraction Scanning Electron Microscopy. Microscopy and Microanalysis, 2016, 22, 488-489.	0.2	1
50	Comparison of energy filtered TEM spectra image and automated crystal orientation mapping in LiFePO 4 phase mapping. Microscopy and Microanalysis, 2016, 22, 1296-1297.	0.2	1
51	4D-STEM Pair Distribution Function Mapping of the Morphology and Structure of Amorphous Organic Materials. Microscopy and Microanalysis, 2019, 25, 1944-1945.	0.2	1
52	Understanding Structure Changes during Cycling of MoS2-based Mg Batteries. Microscopy and Microanalysis, 2019, 25, 2042-2043.	0.2	0
53	4D-STEM: Combining Pair Distribution Mapping and Multivariate Statistic Analysis to Quantify Structures in Complex Nanoscale Glasses. Microscopy and Microanalysis, 2021, 27, 1788-1790.	0.2	0